https://doi.org/10.1007/s41230-023-2015-8

Microstructure and mechanical properties of a cast heat-resistant rare-earth magnesium alloy

Xiao-ping Zhu[1], Jun-qing Yao[2], Hai-long Wu[3, 4], *Xin-wang Liu[2], Hua Liu[5], Zi-tian Fan[2], Shu-lin Lü[2], **Kai Wang[3, 4], and Zi-dong Wang[1]

1. School of Materials Science and Engineering, University of Science and Technology Beijing, Beijing 100083, China
2. State Key Laboratory of Materials Processing and Die & Mould Technology, School of Materials Science and Engineering, Huazhong University of Science and Technology, Wuhan 430074, China
3. Dekai Intelligent Casting Co., Ltd., Zhuozhou 072750, Hebei, China
4. China Iron and Steel Research Institute Group, Beijing 100081, China
5. Guangdong Hongtu Wuhan Die-casting Co., Ltd., Wuhan 430207, China

Abstract: Microstructure, mechanical properties and phase transformation of a heat-resistant rare-earth (RE) Mg-16.1Gd-3.5Nd-0.38Zn-0.26Zr-0.15Y (wt.%) alloy were investigated. The as-cast alloy is composed of equiaxed α-Mg matrix, net-shaped Mg_5RE and Zr-rich phases. According to aging hardening curves and tensile properties variation, the optimized condition of solution treatment at 520 °C for 8 h and subsequent aging at 204 °C for 12 h was selected. The continuous secondary Mg_5RE phase predominantly formed at grain boundaries during solidification transforms to residual discontinuous β-Mg_5RE phase and fine cuboid REH_2 particles after heat treatment. The annealed alloy exhibits good comprehensive tensile property at 350 °C, with ultimate tensile strength of 153 MPa and elongation to fracture of 6.9%. Segregation of RE elements and eventually RE-rich precipitation at grain boundaries are responsible for the high strength at elevated temperature.

Keywords: heat-resistant magnesium alloy; rare earth; microstructure; phase transformation; tensile property; strengthening

CLC numbers: TG146.22 **Document code:** A **Article ID:** 1672-6421(2023)04-289-10

1 Introduction

Magnesium (Mg) alloys have attracted considerable attention in the fields of aerospace applications owing to its excellent creep resistance, high specific strength and low density [1-4]. Nevertheless, such alloys are restricted for the poor heat-resistance and the low absolute strength. There is an increasing interest in rare earth (RE) containing Mg alloys due to their higher mechanical performance than conventional Mg-Al or Mg-Zn series alloys at room and elevated temperatures [5-8]. In this respect, Mg-Gd and Mg-Y alloy systems, such as Mg-Gd-Y-Zr [9], Mg-Gd-Y-Zn [10], Mg-Gd-Y-Nd-Zr [11], Mg-Gd-Y-Zn-Zr [12], have been extensively researched. The addition of element Gd to Mg alloys leads to lattice distortion, which can appreciably enhance yield strength [13, 14]. On this basis, element Y addition will further strengthen the alloy [15]. In contrast to Gd or Y, Nd has a lower solubility of 3.6wt.% at the eutectic temperature, and element Nd addition in the Mg-Gd/Y based alloys can give rise to improvement of mechanical properties by enhancing the precipitation and dispersion strengthening [16, 17]. Besides, Zn element addition in Mg-Gd/Y based alloys leads to the formation of lamellar phases, which is able to enhance the resultant alloys by means of short-fiber strengthening [18-20]. Grain refinement is also an important method to improve both the strength and ductility. For instance, Zr element is an effective grain refiner of Mg alloys by promoting heterogeneous nucleation and constitutional supercooling [21]. Hence, Mg-Gd-Nd-Y-Zr-Zn alloys are supposed to exhibit remarkable mechanical properties, which can be a promising candidate for producing high strength Mg alloys.

In general, complex Mg alloy components are fabricated by casting, one of the fundamental

***Xin-wang Liu**

Male, born in 1982, Ph.D, Professor. His research interests mainly focus on as-cast microstructure refinement, strengthening, and phase transformation of magnesium, aluminum, titanium, and high-entropy alloys.

E-mail: liuxw@hust.edu.cn

****Kai Wang**

E-mail: wangkai483@aliyun.com

Received: 2022-08-08; Accepted: 2023-01-12

techniques [14]. This process involves considerations such as melt cleanliness, castability, defect removal, and uniformity in microstructure, grain size and properties. Furthermore, numerous reports on heat treatment of cast Mg alloys [22-25] have shown that appropriate solid solution and aging processes can significantly improve mechanical properties by reducing casting defects and obtaining desired precipitates. Conventional T6 heat treatment is considered to be effective in modifying the microstructure and mechanical properties of the as-cast WE43 Mg alloy [26], but has no obvious effect on the WE43 Mg alloy obtained by selective laser melting [27]. Therefore, appropriate heat treatment conditions should be designed when developing new alloy systems, considering the unique microstructure of Mg alloys with different compositions or processed using different methods.

Although previous studies have investigated Mg-RE-Zn-Zr alloys containing certain RE elements, there is still a lack of detailed descriptions regarding alloys with hidh RE contents and theri high temperature performance. Additionally, there is a limited understanding of the strengthening mechanism and its implications for alloy properties. Therefore, a heat-resistant Mg-16.1Gd-3.5Nd-0.38Zn-0.26Zr-0.15Y (wt.%) alloy with high Gd and Nd content was chosen in the present study. An attempt was made in this study to describe the microstructure of this heat-resistant Mg alloy after heat treatment and assess its link to mechanical properties.

2 Experimental procedure

The as-cast Mg-16.1Gd-3.5Nd-0.38Zn-0.26Zr-0.15Y (wt.%) alloy was prepared by melting the commercial pure Mg ingot (> 99.9%), pure Zn particles (99.9%), and Mg-30Gd (wt.%), Mg-25Nd (wt.%), Mg-30Zr (wt.%), Mg-30Y (wt.%) master alloys under the mixture of CO_2 and SF_6 shielding gas. The actual chemical compositions were examined by X-ray fluorescence (XRF, a SHIMADZU XRF-1800 spectroscope). After melting pure Mg in an electric resistance furnace at 750 °C, pure Zn and master alloys pre-heated at 200 °C were added to the molten Mg. Then, the melt was poured into a cube copper mold pre-heated at 200 °C with dimensions of Φ70 mm×160 mm. After being machined into 10 mm×10 mm×40 mm rectangular blocks, samples were heat treated at 520 °C for 8 h followed by quenching in water at 66 °C. Finally, the Mg-RE alloys were subjected to air cooling after aging at 204 °C for 1, 12, 36, 48, 96, 120 and 160 h, respectively.

The samples for phase analysis and microstucture observation were cut by electric discharge machining (EDM) from the as-cast ingot and heat-treatment sheets and then ground with SiC adhesive papers to a grit size of 7 μm and polished with diamond suspension down to 1 μm. After mechanical polishing, constitution and microstructure of the alloys were investigated using X-ray diffraction (XRD) and scanning electron microscopy (SEM) and transmission electron microscopy (TEM) techniques. The XRD analysis was performed using a SHIMADZU XRD-7000S diffractometer using Cu Kα radiation (λ=1.54 Å) with the range of 10°–80° at a speed of 5°·min^{-1}. Microchemical and morphological characterizations were conducted utilizing an FEI Quanta 200 microscope operated at the back-scatter electron (BSE) and secondary electron (SE) modes equipped with an energy dispersive X-ray spectroscope (EDS) at an accelerating voltage of 20 kV, similar to our previous procedures [28]. The samples for SEM microstructure observation were chemically etched with a solution of ethanol and nitric with a volume ratio of 24:1. Specimens for TEM analysis were ground down to foils with a thickness of about 50 μm using fine SiC papers, and discs with a diameter of 3 mm were punched out of the foils, followed by dimpling and finally ion milling. Finally, TEM investigations were performed using an FEI Tecnai G2 F30 microscope operated at an accelerating voltage of 200 kV or 300 kV.

Specimens for tensile tests were also cut by EDM and the tensile tests were performed on a SHIMADZU AG-100 kN testing machine at an engineering strain rate of 10^{-3} s^{-1} in air at 350 °C. The specimens were firstly put in the machine and heated to 350 °C and held for 5 min to get a uniform temperature distribution before the tensile testing. The Vickers hardness testing was performed on a HV-1000 microhardness tester.

3 Results

3.1 Microstructures

The microstructure of as-cast Mg-16.1Gd-3.5Nd-0.38Zn-0.26Zr-0.15Y alloy shown in Fig. 1(a) exhibits typical equiaxed grains with an average grain size of about 50 μm. The SEM-BSE microstructures in Fig. 1(b) indicate that the alloy is composed of α-Mg matrix and three types of secondary phase: net-shaped phases denoted as Region 2, continuous ones in grain boundaries (GBs) as Region 3, and isolated phase in the interior of the matrix as Region 4. The elemental distribution of Fig. 1(b) is shown in Figs. 1(c–h). As can be seen, the as-cast alloy exhibits compositional fluctuation in tens of micrometer scale because of the solute redistribution during solidification. The primary grains are enriched in Mg and Gd, whereas GBs are enriched in Nd, and the secondary phases are Zr-rich, whereas Y and Zn are uniformly distributed, which can be distinguished from their contrasts.

The eutectic is composed of α-matrix and intermetallic compounds. For quantitative analysis, chemical compositions of different regions marked in Fig. 1(b) analyzed by EDS are listed in Table 1. The results indicate that the matrix is mainly composed of Mg, which is as same as the study of Ref. [29]. The GBs eutectic containing net-shaped phase (Region 2) and continuous phase (Region 3) is rich in RE, especially Gd and Nd. It has been reported that RE elements blend with each other in Mg-Gd-Y alloys, forming $Mg_5(Gd_{1-x}Y_y)$ compound, which should be attributed to the similarity between the RE element [30]. Compounds in this work are similar to those of previous research [31-33], which could be identified as Mg_5RE (RE=Gd, Nd, Y) phase, while Zn exists at solid solution state.

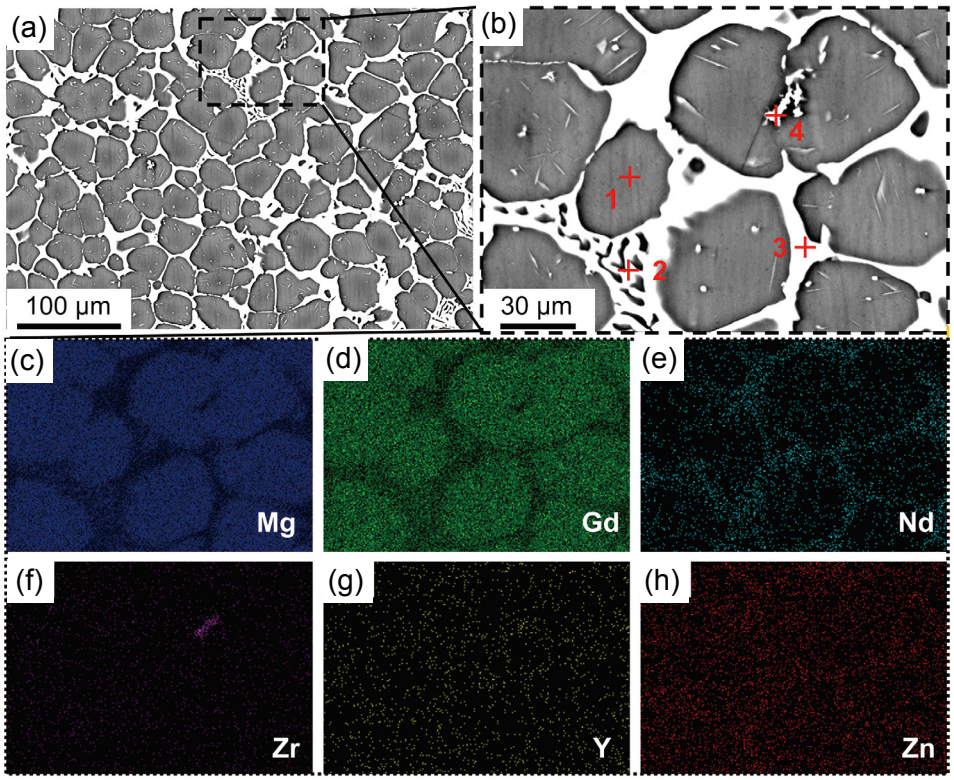

Fig. 1: Microstructures of as-cast Mg-16.1Gd-3.5Nd-0.38Zn-0.26Zr-0.15Y alloy: (a) representative SEM-BSE images with low-magnification; (b) high-magnification showing equiaxed α-Mg grains surrounded by eutectic structures of Mg_5RE; (c–h) corresponding elemental EDS maps of Mg (c), Gd (d), Nd (e), Zr (f), Y (g), Zn (h), respectively

Table 1: Chemical compositions of selected regions in Fig. 1(b) of as-cast Mg-16.1Gd-3.5Nd-0.38Zn-0.26Zr-0.15Y alloy tested by SEM-EDS

Region	Composition (at.%)						Phase
	Mg	Gd	Nd	Zr	Y	Zn	
1	98.49	0.97	0.54	–	–	–	α-Mg
2	88.99	7.59	2.52	–	0.16	0.73	Mg_5RE
3	90.81	5.11	2.48	0.08	0.23	1.29	Mg_5RE
4	58.30	3.46	0.95	35.03	1.67	0.59	Zr-rich

The isolated phase (Region 4) is composed of a large amount of Zr, which plays a role in heterogeneous nucleation and grain refinement [34]. The XRD pattern of the as-cast alloy in Fig. 2 shows peaks corresponding to α-Mg and Mg_5RE phases. The results are consistent with the aforementioned chemical composition analysis of each phase. However, it should be noted that the phase enriched in Zr, not detected by XRD, indeed exists in the alloy. This is probably because of its small volume fraction and the limited particle size.

3.2 Aging response

Figure 3(a) shows the age-hardening curve of the solution treated alloys aged at 204 °C for different aging times. At the initial stages of the aging, the hardness increases with the increase of aging time until it reaches the peak hardness.

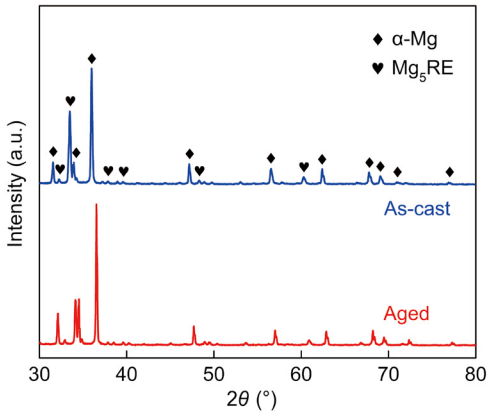

Fig. 2: X-ray diffraction patterns of as-cast and aged Mg-16.1Gd-3.5Nd-0.38Zn-0.26Zr-0.15Y alloys

However, the hardness gradually decreases as a result of over-aging. The specimen aged at 204 °C for 48 h exhibits the highest hardness of 160.1 HV. Similar to conventional cast Mg-Gd series alloys [32], aging at about 200 °C leads to high hardness increment due to more substantial precipitation potential, but long time (~ 48 h) to reach peak-aged hardness because of slow diffusion of atoms, where the change trend of the hardness corresponds to the precipitation sequence of precipitates during aging. As reported by Peng et al. [30], the microstructure of Mg-12Gd-4Y-2Nd-0.3Zn-0.6Zr alloy at peak hardness aged at 225 °C is composed of Mg_5RE and $Mg_{24}RE_5$ intermetallic compounds. Similar results were reported in WE-type and Mg-Gd-Y alloys [35], in which the metastable phase, identified as β′-$Mg_{15}RE_3$ [36], was observed. The high age hardening response is mainly associated with the formation of metastable precipitates. The relationship between precipitates and the sequence of precipitation will be discussed in the next.

Figure 3(b) shows the variation of the tensile mechanical properties with aging time. Obviously, no distinct age strengthening response is exhibited at selected aging treated stage. The results are different from the Mg-7Gd-5Y-0.6Zn-0.8Zr [37], whose tensile strength increased rapidly after aging time beyond 20 h, however, elongation of the alloys decreased significantly. Actually, both the yield strength (YS) and ultimate tensile strength (UTS) of Mg-16.1Gd-3.5Nd-0.38Zn-0.26Zr-0.15Y alloy do not change drastically after aging for 1, 12 and 48 h, respectively, but the elongation (EL) to fracture achieves peak value after aging for 12 h. Overall, after aging annealing for 12 h, the alloy has better comprehensive properties. Furthermore, whether the above properties governed by the unique microstructure or not have been further studied.

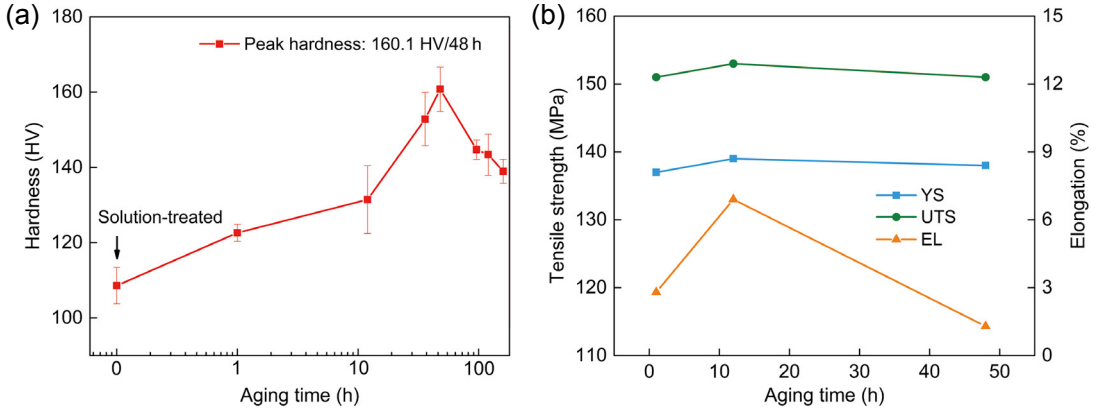

Fig. 3: Aging variations of Mg-16.1Gd-3.5Nd-0.38Zn-0.26Zr-0.15Y alloy after solution treatment and aging at 204 °C for different durations: (a) hardness; (b) mechanical properties

3.3 Aging precipitates

Figure 4 exhibits the SEM-BSE and TEM micrographs of the alloys after solid solution at 520 °C for 8 h and subsequently aging at 204 °C for 12 h. The continuous and net-shaped phases still can be observed. The XRD pattern of the aging alloy in Fig. 2 shows peaks corresponding to α-Mg and Mg_5RE phases, which is similar to the as-cast alloy. Meanwhile, it is noteworthy that a newly cuboid-shaped phase precipitates from the α-matrix and distributes both at GBs and intragranular areas due to the diffusion of elements, as shown in Fig. 4(a).

To ascertain the chemical composition of the second phases in the aged alloy, different regions in Fig. 4(b) were selected for SEM-EDS analysis. The results of Regions B and C listed in Table 2 indicate that the chemical compositions of phases at GBs are close to that of Mg_5RE in as-cast alloy, which can be called β-Mg_5RE. SEM-EDS line scanning marked by inserted line segments in Fig. 4(c) was conducted to estimate the level of elemental fluctuation of the precipitate particles and GB phase, and the results are shown in Figs. 4(d) and (e). The results suggest that the cuboid particles and eutectic phases are evidently enriched in Gd, but depleted in Mg. Selecting the most central point of cuboid particle in Fig. 4(c) to calculate the composition ratio, the contents of those elements except Y are in good agreement with Region D in Fig. 4(b), because the content of Y is too small to be measured precisely, however, both of them can be referred to as RE-rich cuboid phases.

This cuboid phase in Region D enriched in Gd and other RE might be REH_2 reported in the similar Mg-Gd based alloys, where the decomposition of the Mg_5RE intermetallic phase during a solution treatment is found to be the dominating mechanism of the cuboid phase formation [33, 38-40]. Chemical composition of such particle in Ref. [40] was determined by EDS analysis as 86.2at.% Gd and 13.8at.% Mg, which is close to that of the cuboid phase in our work (87.89at.% RE and 10.22at.% Mg). Furthermore, as indicated by the SAD pattern inserted Fig. 4(f), the cuboid particles has major crystallographic orientation similar to that in Ref. [40], which indicate a fcc structure. Therefore, considering that the alloy contains a variety of RE types, this cuboid phase can be identified as REH_2 phase.

Figure 5(a) shows a TEM image of the REH_2 particles and Figs. 5(b–g) show the corresponding EDS maps. At higher magnification, the particles enrich in RE elements (Gd, Nd, Y) and slightly lack in Mg. While elemental segregation of the other regions is not so evident. An essential difference of the elemental contents in the microstructure between

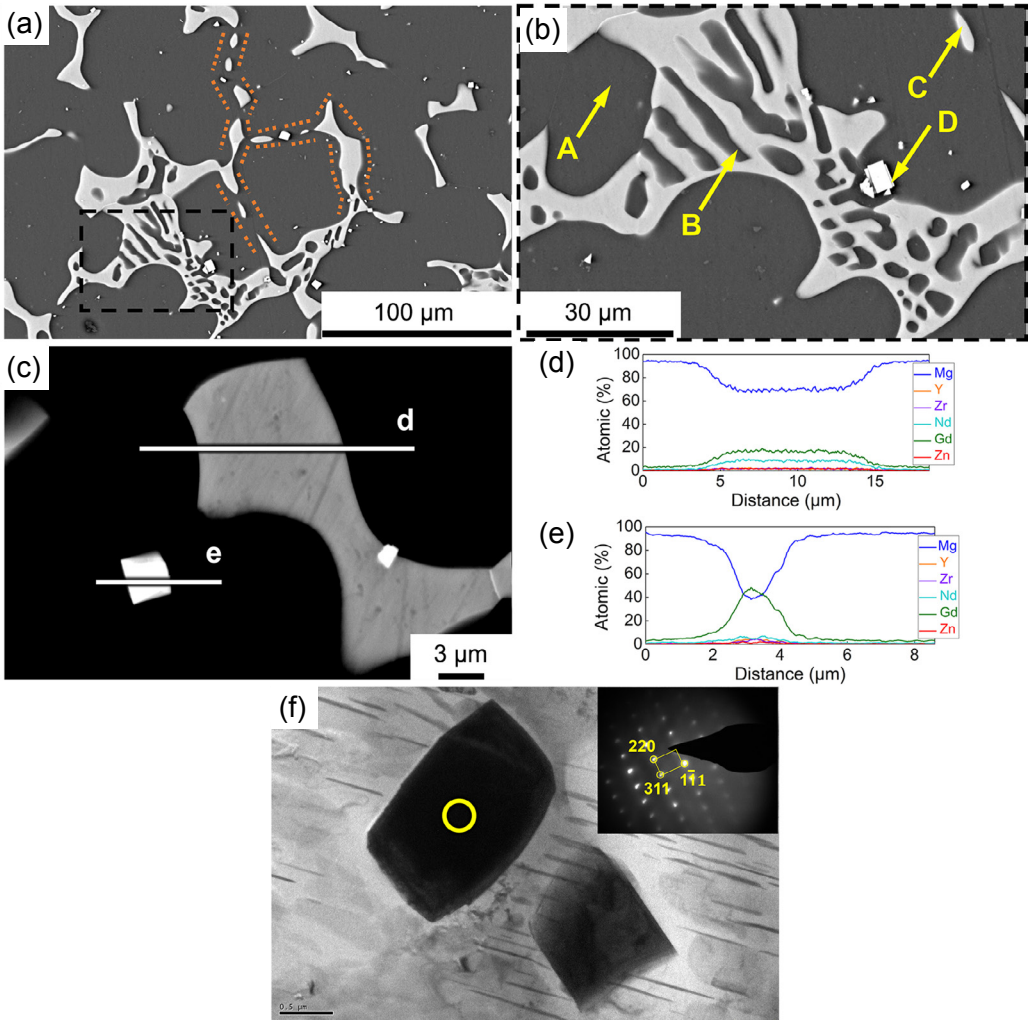

Fig. 4: SEM-BSE and TEM microstructure of Mg-16.1Gd-3.5Nd-0.38Zn-0.26Zr-0.15Y alloy after aging heat treatment: representative SEM-BSE images with low-magnification (a) and high-magnification (b); EDS lines scanning along the white lines in (c) and results displayed in (d) and (e); TEM microstructure of cuboid particles and corresponding SAD pattern inserted (f)

Table 2: Chemical compositions of selected regions in Fig. 4(b) of aged Mg-16.1Gd-3.5Nd-0.38Zn-0.26Zr-0.15Y alloy tested by SEM-EDS

Region	Composition (at.%)						Phase
	Mg	Gd	Nd	Zr	Y	Zn	
A	96.71	2.52	0.53	0.15	0.09	–	α-Mg
B	86.17	8.80	3.72	0.12	0.19	1.0	Mg_5RE
C	84.89	9.49	4.12	0.20	0.15	1.15	Mg_5RE
D	10.22	51.32	3.23	0.98	33.34	0.91	RE-rich

as-cast alloy and aging heat-treatment alloy positively proves the transition of phases. Furthermore, it should be noted that metastable precipitations formed in the aged alloys, and the precipitations are morphologically approximate to β″ and β′ in Ref. [41]. The β″ phase has a lenticular-shaped morphology, while the β′ has a discontinuous rod type according to Ref. [42]. Besides, it is reported that the precipitation in the Mg-Gd-Y-Zn-Zr alloys aged at 210 °C generally proceeds with an order of Mg (S.S.S.S) → β″ (DO_{19}) → β′ (bco) → $β_1$ (fcc) [37]. When the sample is over-aged (~ 160 h), in order to minimize the shear strain around the β′ phase, rhombic $β_1$ phase would precipitate invariably [37]. Considering that Mg-16.1Gd-3.5Nd-0.38Zn-0.26Zr-0.15Y alloy has not been over-aged, it is highly possible that the lenticular-shaped phase and rod-type phase are β″ and β′, respectively.

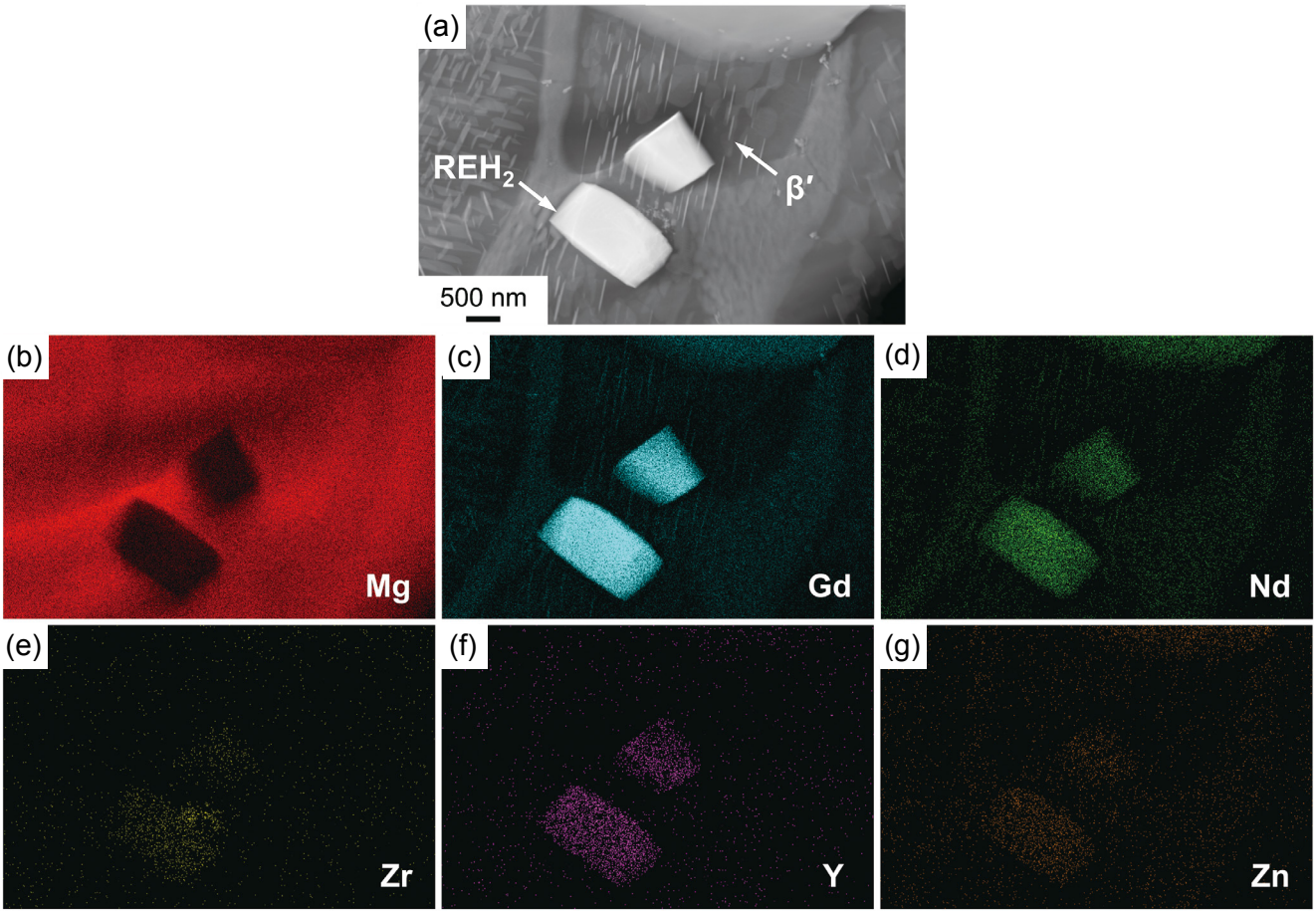

Fig. 5: TEM and elemental EDS maps of aged Mg-16.1Gd-3.5Nd-0.38Zn-0.26Zr-0.15Y alloy: (a) cuboid particles; (b–g) elemental EDS maps of Mg (b), Gd (c), Nd (d), Zr (e), Y (f), Zn (g) in (a)

3.4 Mechanical properties

Figure 6 presents the representative high temperature tensile engineering stress-strain curves of the Mg-16.1Gd-3.5Nd-0.38Zn-0.26Zr-0.15Y alloys under different states tested at 350 °C. The tensile strength and elongation differ substantially from each state. It can be seen from Fig. 6 that the aged alloy exhibits enhanced properties than the as-cast alloy. The yield strength (YS), ultimate tensile strength (UTS) and elongation to fracture (EL) of the as-cast alloy are 102 MPa, 122 MPa and 1.7%, respectively. Subsequent aging treatment evidently strengthens the alloy, leading to YS of 139 MPa and UTS of 153 MPa, and a significant improvement of the EL to 6.9%. The aged Mg-16.1Gd-3.5Nd-0.38Zn-0.26Zr-0.15Y alloy shows fairly better comprehensive high temperature tensile performance than Mg-13Gd-2Y-0.5Zr and Mg-15Gd alloys in Refs. [43, 44].

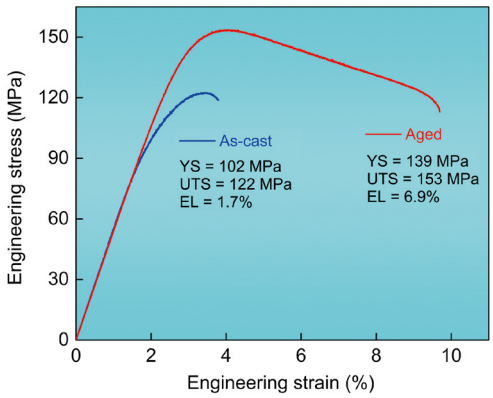

Fig. 6: Representative tensile engineering stress-strain curves of as-cast and after 12 h age-treated Mg-16.1Gd-3.5Nd-0.38Zn-0.26Zr-0.15Y alloys at 350 °C

The fractographic analysis of the ruptured surfaces of tensile specimens was conducted to determine the fracture mechanism. Figure 7 shows the high-temperature tensile fracture morphologies of the alloys under as-cast and aging conditions. The fracture surface of the as-cast alloy indicates that the pores (remarked by red arrows) and cracks (remarked by blue arrows) in Fig. 7(a) can be associated with Mg_5RE phase (remarked by white arrows) in Fig. 7(b). A close-up view inserted in Fig. 7(a) shows clear crack shape. It can be responsible for premature fracture during the tensile test and is consistent with very low EL of the as-cast alloy [45]. Conversely, for microstructures after aging heat treatment in Figs. 7(c) and (d), the fracture surface exhibits dimples-like features remarked by yellow arrows and particles remarked by orange arrows in Fig. 7(c). This suggests that the decohesion between the eutectic and the particle is contributing to a significant improvement of EL [44, 46].

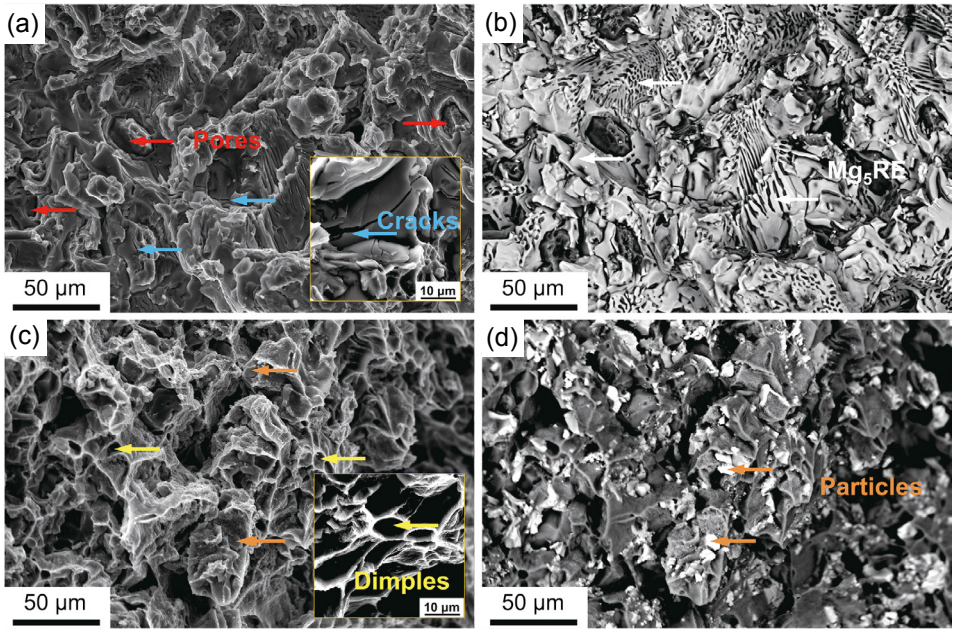

Fig. 7: Tensile fracture SEM images of as-cast (a, b) and aged (c, d) Mg-16.1Gd-3.5Nd-0.38Zn-0.26Zr-0.15Y alloys at 350 °C: (a, c) SE mode; (b, d) BSE mode

4 Discussion

In the light of previous research [47, 48] on solidification, accumulated solutes would increase the driving force for the diffusion of the solute at the dendrite tip, and it has been suggested that the liquid concentration at solid/liquid interface can affect the supersaturation, Ω, as shown in Eq. (1):

$$\Omega = \frac{C_L^* - C_0}{C_L^* - C_S^*} = \frac{1 - C_0 / C_L^*}{1 - k_0} \quad (1)$$

where C_0 is the initial concentration of the alloy, C_L^* and C_S^* are the liquid and solid concentration at the solid/liquid interface, respectively, and k_0 is the equilibrium partition coefficient. Equation (1) reveals the driving force for the diffusion-controlled growth is a monotonic increasing function of the liquid concentration at the solid/liquid interface during solidification.

In this work, the net-shaped Mg_5RE secondary phase is formed during non-equilibrium solidification. When the temperature is descending to the eutectic point, the liquid phase approaches its eutectic composition due to k_0<1 and negligible diffusivity in solid. Thus, a non-equilibrium eutectic structure is formed at GBs, which are generally the last solidification regions. Furthermore, with the increment of RE contents, their effect on crystal grain refinement is mainly attributed to constitutional supercooling [49]. The lattice parameters of the coarse eutectics enriched in RE and distributed along GBs are different from those of the α-Mg matrix, and there are phase boundaries between the two phases. Meanwhile, the eutectics with irregularly net-shape and sharp edge may cause stress concentration under loading [50]. Therefore, microcracks form in the eutectics, resulting in a low ductility of as-cast alloy. Actually, in metals and alloys, GBs and phase interfaces contain lots of defects such as dislocations and vacancies, along which the diffusion ocurrs easier and faster.

It is reported that [32] the net-shaped phases appeared at as-cast state were transformed to a spheroidized β-Mg_5RE phase and a cuboid REH_2 phase during the solid solution procedure. After subsequent aging heat treatment, the former is partly dissolved, but the latter is still remained owing to its high thermostability. The precipitation behavior of the REH_2 cuboid phase in this work is analogous to the cuboid GdH_2 [40] and DyH_2 [51], and the transformation process of the REH_2 phase is schematically illustrated in Fig. 8. In the initial stage, concaves and convexities are observed on the particles along the interface, indicating different stress status, as shown in Fig. 8(a). The adjacent RE atoms escape from the Mg_5RE lattice along the direction marked by arrows and move by chance due to the interface tension. As a consequence, the RE atoms diffuse along the interfaces and come into the magnesium lattice at a new location, leading to the local decomposition and morphology discontinuity of the β-Mg_5RE phase, as indicated in Fig. 8(b). Then, the atoms at the tip would move towards the middle, which makes the concaves hollow, and the convexities smoother. Over time, it is assumed that the smooth part of the particle keeps stable due to the homogenous diffusion along the interface. Meanwhile, near the concaves continuous net-shaped Mg_5RE will be severed and the spheroidization of the sub-particles will continue, as shown in Fig. 8(c). Finally, the Mg_5RE phase is partly dissolved, resulting in presence of some spheroidal β-Mg_5RE phases and REH_2 cuboid-shaped particles in aged alloys, as shown in Fig. 8(d).

The strengthening of high temperature tensile properties by aging heat treatment can be mainly ascribed to several aspects. Primarily, the high solid solution of the RE elements plays an important role in the enhancement of mechanical properties. The stress generated by larger RE elements atoms entering the Mg matrix during dissolution can roughen the slip plane

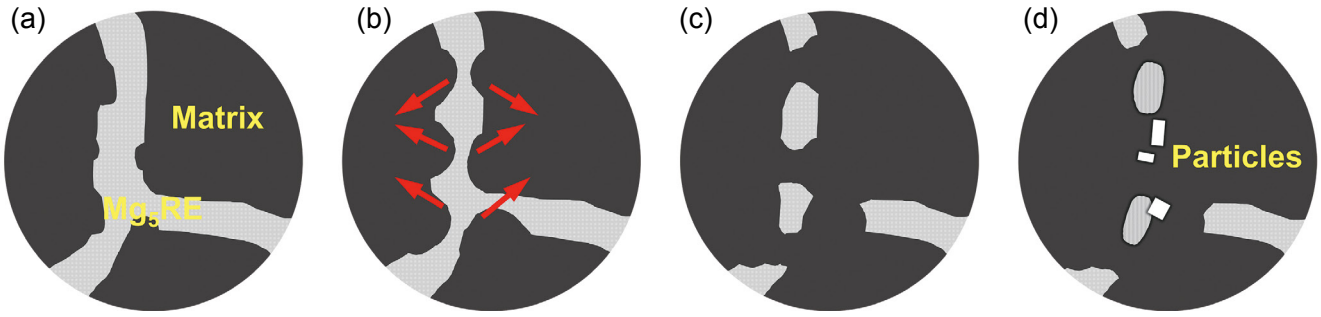

Fig. 8: Simplified schematic drawing of transformation procedure of Mg_5RE phase: (a) initial stage of phases; (b) concaves and necking of phase; (c) discontinuity and fragmentized of phase; (d) partly dissolved phase and residual Mg_5RE and cuboid-shaped REH_2. The arrow indicates the moving direction of RE atoms

and impede dislocation movement, thus the resistance against dislocation motion is improved, leading to the increment of the yield strength. Generally, the spacing of dissolved atoms on the slip plane varies as $C^{-1/2}$ (C is solid solution concentration). As a result, the dislocation yield strength increases with solute concentration [30]. Meanwhile, the existence of stable dispersed RE-rich precipitates in GBs can effectively hinder basal plane slip at elevated temperature due to their high melting point. The phases change their orientation to inhibit the deformation of α-Mg matrix at a certain temperature, especially at elevated temperatures [52]. Analogously, both the metastable β′ precipitate and REH_2 exhibit semi-coherent structure with Mg matrix, which can effectively prevent sliding of basal plane [53, 54]. However, with the increase of aging time, the precipitates can change the semi-coherent crystal lattice, which decreases the strengthening effect. Furthermore, β′ metastable phase has also been identified in the decomposition sequence before β phases and is also considered as one of the strengthening precipitates, for instance, in Mg-4Y-2.25Nd-0.6Zr and Mg-7(Gd/Dy)-2.25Nd-0.6Zr alloys [55, 56]. The improved mechanical properties are mainly ascribed to the coexistence of metastable β′ phases and REH_2 particles precipitations, as well as the decrease of stable Mg_5RE phase.

It is more important to note that elongation to fracture of the alloy after aging heat treatment has a remarkable increment from 1.7% to 6.9%. The high ductility mainly associates with fine precipitations phases. Mg with an HCP structure, has only basal slip system at low temperatures due to much higher critical resolved shearing stress (CRSS) in cylinder and conical slip. This slip system is active during plastic deformation, leading to poor ductility [57]. The fine β′ precipitates can effectively hinder dislocation gliding and would not induce serious stress concentration in the nearby phases to form micro-crack. The blending addition of RE elements distinctly ameliorates mechanical properties, which means large grains deform and a great number of dislocations entwisted at grain boundaries will improve the plasticity more effectively [57]. In other words, the precipitates distributed along GBs can hinder GBs of the alloy gliding and coordinate deformation between grains, which is conducive to improving the ductility of the aged alloys.

5 Conclusions

The microstructure and mechanical properties of Mg-16.1Gd-3.5Nd-0.38Zn-0.26Zr-0.15Y alloy at as-cast and aged states were characterized and analyzed. The conclusions can be drawn as following:

(1) The as-cast microstructure mainly consists of equiaxed grains (α-Mg), net-shaped eutectic structure (Mg_5RE) at GBs, and Zr-rich phase inside the grain. After aging heat treatment, the net-shaped eutectic structure Mg_5RE is partly resolved, and the cuboid REH_2 particles are formed at GBs, and a large number of metastable phases β′ are uniformly distributed at the interior of the Mg matrix.

(2) The tensile strength and elongation of as-cast alloy at 350 °C are 122 MPa and 1.7%, respectively. Aging heat treatment leads to an evidently enhancement in both strength and ductility to 153 MPa and 6.9%, respectively.

(3) The fracture mechanism and resultant morphology of the tensile samples depend on the content and shape of Mg_5RE in the microstructure. For the as-cast alloy, the intercrystalline cracks and pores of the eutectic are accompanied by the large Mg_5RE over the surface of rupture. The reduction of Mg_5RE and existence of RE-rich precipitation is a key factor controlling the tensile properties of an aged alloy.

Acknowledgement

The authors would like to thank the support of the National Natural Science Foundation of China (Grant number 52071088).

Conflict of interest

The authors declare no financial and personal relationships with other people or organizations that can inappropriately influence our work, there is no professional or other personal interest of any nature or kind in any product, service and/or company that could be construed as influencing the position presented in, or the review of, the manuscript submitted.

References

[1] Kim Y J, Kim S H, Lee J U, et al. Effects of cold pre-forging on microstructure and tensile properties of extruded AZ80 alloy. Materials Science and Engineering: A, 2017, 708: 405–410.
[2] Cai Z, Chen F, Guo J. Constitutive model for elevated temperature flow stress of AZ41M magnesium alloy considering the compensation of strain. Journal of Alloys and Compounds, 2015, 648: 215–222.
[3] Mordike B L, Ebert T. Magnesium: Properties-applications-potential. Materials Science and Engineering: A, 2001, 302(1): 37–45.
[4] Kaiser M S, Datta S, Roychowdhury A, et al. Age hardening behavior of wrought Al-Mg-Sc alloy. Materials and Manufacturing Processes, 2007, 23(1): 74–81.
[5] Li J, Chen R, Ma Y, et al. Characterization and prediction of microporosity defect in sand cast WE54 alloy castings. Materials Science & Technology, 2014, 30(10): 991–997.
[6] Wang J, Meng J, Zhang D, et al. Effect of Y for enhanced age hardening response and mechanical properties of Mg-Gd-Y-Zr alloys. Materials Science and Engineering: A, 2007, 456(1): 78–84.
[7] Yang Y, Yang M, He C, et al. Rare earth improves strength and creep resistance of additively manufactured Zn implants. Composites, Part B: Engineering, 2021, 216: 108882.
[8] Masoudpanah S M, Mahmudi R. Effects of rare-earth elements and Ca additions on the microstructure and mechanical properties of AZ31 magnesium alloy processed by ECAP. Materials Science and Engineering: A, 2009, 526(1): 22–30.
[9] Zhou H, Cheng G M, Ma X L, et al. Effect of Ag on interfacial segregation in Mg-Gd-Y-(Ag)-Zr alloy. Acta Materialia, 2015, 95: 20–29.
[10] Garces G, Máthis K, Barea R, et al. Effect of precipitation in the compressive behavior of high strength Mg-Gd-Y-Zn extruded alloy. Materials Science and Engineering: A, 2019, 768: 138452.
[11] Li Y, Qu C, Wang J, et al. Exceptional aging hardening behaviour of nanocrystalline Mg-Y-Nd-Gd-Zr alloy prepared by high pressure torsion. Journal of Alloys and Compounds, 2020, 813: 152123.
[12] Xu C, Nakata T, Fan G H, et al. Enhancing strength and creep resistance of Mg-Gd-Y-Zn-Zr alloy by substituting Mn for Zr. Journal of Magnesium and Alloys, 2019, 7(3): 388–399.
[13] Liu Q, Ding X, Liu Y, et al. Analysis on micro-structure and mechanical properties of Mg-Gd-Y-Nd-Zr alloy and its reinforcement mechanism. Journal of Alloys and Compounds, 2017, 690: 961–965.
[14] Wu G, Wang C, Sun M, et al. Recent developments and applications on high-performance cast magnesium rare-earth alloys. Journal of Magnesium and Alloys, 2021, 9(1): 1–20.
[15] Jiang R, Qian S, Dong C, et al. Composition optimization of high-strength Mg-Gd-Y-Zr alloys based on the structural unit of Mg-Gd solid solution. Journal of Materials Science & Technology, 2021, 72: 104–113.
[16] Peng Q, Wu Y, Fang D, et al. Microstructures and mechanical properties of Mg-8Gd-0.6Zr-*x*Nd (*x*=0, 1, 2 and 3 mass%) alloys. Journal of Materials Science, 2007, 42(11): 3908–3913.
[17] Massalski T, Okamoto H, Subramanian P, et al. Binary alloy phase diagrams. ASM International, 1986.
[18] Hagihara K, Kinoshita A, Sugino Y, et al. Effect of long-period stacking ordered phase on mechanical properties of Mg97Zn1Y2 extruded alloy. Acta Materialia, 2010, 58(19): 6282-6293.
[19] Hagihara K, Yokotani N, Umakoshi Y. Plastic deformation behavior of Mg12YZn with 18R long-period stacking ordered structure. Intermetallics, 2010, 18(2): 267–276.
[20] Zhou H, Liu K, Zhang L, et al. Influence of high pressure during solidification on the microstructure and strength of Mg-Zn-Y alloys. Journal of Rare Earths, 2016, 34(4): 435–440.
[21] Ma Q, StJohn D H, Frost M T. Characteristic zirconium-rich coring structures in Mg-Zr alloys. Scripta Materialia, 2002, 46(9): 649–654.
[22] Li J, He Z, Fu P, et al. Heat treatment and mechanical properties of a high-strength cast Mg-Gd-Zn alloy. Materials Science and Engineering: A, 2016, 651: 745–752.
[23] Ozaki T, Kuroki Y, Yamada K, et al. Mechanical properties of newly developed age hardenable Mg-3.2 mol%Gd-0.5 mol%Zn casting alloy. Materials Transactions, 2008, 49(10): 2185–2189.
[24] Zhang Y, Wu Y, Peng L, et al. Microstructure evolution and mechanical properties of an ultra-high strength casting Mg-15.6Gd-1.8Ag-0.4Zr alloy. Journal of Alloys and Compounds, 2014, 615: 703–711.
[25] Zhang J, Leng Z, Liu S, et al. Microstructure and mechanical properties of Mg-Gd-Dy-Zn alloy with long period stacking ordered structure or stacking faults. Journal of Alloys and Compounds, 2011, 509(29): 7717–7722.
[26] Jahedi M, McWilliams B A, Knezevic M. Deformation and fracture mechanisms in WE43 magnesium-rare earth alloy fabricated by direct-chill casting and rolling. Materials Science and Engineering: A, 2018, 726: 194–207.
[27] Hyer H, Zhou L, Benson G, et al. Additive manufacturing of dense WE43 Mg alloy by laser powder bed fusion. Additive Manufacturing, 2020, 33: 101123.
[28] Yin Z, Liu X, Gao N, et al. Grain refinement of a NiCoFe medium entropy alloy: Composition design from solute interaction perspective. Journal of Alloys and Compounds, 2023, 951: 169966.
[29] Wang J, Liu R, Dong X, et al. Microstructure and mechanical properties of Mg-Zn-Y-Nd-Zr alloys. Journal of Rare Earths, 2013, 31(6): 616–621.
[30] Peng Q, Hou X, Wang L, et al. Microstructure and mechanical properties of high performance Mg-Gd based alloys. Materials & Design, 2009, 30(2): 292–296.
[31] Liu X, Zhang Z, Le Q, et al. Effects of Nd/Gd value on the microstructures and mechanical properties of Mg-Gd-Y-Nd-Zr alloys. Journal of Magnesium and Alloys, 2016, 4(3): 214–219.
[32] Yu Z, Xu C, Meng J, et al. Microstructure evolution and mechanical properties of as-extruded Mg-Gd-Y-Zr alloy with Zn and Nd additions. Materials Science and Engineering: A, 2018, 713: 234–243.
[33] Gao Y, Wang Q, Gu J, et al. Behavior of Mg-15Gd-5Y-0.5Zr alloy during solution heat treatment from 500 to 540 °C. Materials Science and Engineering: A, 2007, 459(1): 117–123.
[34] Qian M, Stjohn D H, Frost M T. Characteristic zirconium-rich coring structures in Mg-Zr alloys. Scripta Materialia, 2002, 46(9): 649–654.
[35] Antion C, Donnadieu P, Perrard F, et al. Hardening precipitation in a Mg-4Y-3RE alloy. Acta Materialia, 2003, 51(18): 5335–5348.
[36] Honma T, Ohkubo T, Hono K, et al. Chemistry of nanoscale precipitates in Mg-2.1Gd-0.6Y-0.2Zr (at.%) alloy investigated by the atom probe technique. Materials Science and Engineering: A, 2005, 395(1–2): 301–306.
[37] Jin X, Xu W, Li K, et al. Influence of heat treatment on the evolution of microstructure and mechanical properties of Mg-7Gd-5Y-0.6Zn-0.8Zr magnesium alloy. Materials Science and Engineering: A, 2018, 729: 219–229.
[38] Alizadeh R, Mahmudi R, Ngan A H W, et al. An unusual extrusion texture in Mg-Gd-Y-Zr alloys. Advanced Engineering Materials, 2016, 18(6): 1044–1049.

[39] Yang Z, Wang Z H, Duan H B, et al. Microstructure evolution of Mg-6Gd-2Y alloy during solid solution and aging process. Materials Science and Engineering: A, 2015, 631: 160–165.
[40] Vlček M, Čížek J, Lukáč F, et al. Hydrogen absorption in Mg-Gd alloy. International Journal of Hydrogen Energy, 2017, 42(35): 22598–22604.
[41] Jun J H, Seong K D, Lee M H. Effect of Zirconium on high temperature tensile properties of precipitation-hardened Mg-Nd-Zn casting alloy. International Journal of Modern Physics B, 2009, 23(6): 966–971.
[42] Zheng K, Dong J, Zeng X, et al. Precipitation and its effect on the mechanical properties of a cast Mg-Gd-Nd-Zr alloy. Materials Science and Engineering: A, 2008, 489(1–2): 44–54.
[43] Chen X, Li Q, Zhu L, et al. Abnormal temperature effect on tensile strength of Mg-13Gd-2Y-0.5Zr alloy. Vacuum, 2020, 177: 109398.
[44] Ouyang S, Yang G, Qin H, et al. Effect of the precipitation state on high temperature tensile and creep behaviors of Mg-15Gd alloy. Journal of Magnesium and Alloys, 2022, 10(12): 3459–3469.
[45] Deng Q, Wu Y, Zhu W, et al. Effect of heat treatment on microstructure evolution and mechanical properties of selective laser melted Mg-11Gd-2Zn-0.4Zr alloy. Materials Science and Engineering: A, 2022, 829: 142139.
[46] Czerwinski F, Zielinska-Lipiec A, Pinet P J, et al. Correlating the microstructure and tensile properties of a thixomolded AZ91D magnesium alloy. Acta Materialia, 2001, 49(7): 1225–1235.
[47] Fu J W, Yang Y S. Formation of the solidified microstructure of Mg-Al-Zn alloy under a low-voltage pulsed magnetic field. Journal of Materials Research, 2011, 26(14): 1688–1695.
[48] Fisher D, Kurz W. Fundamentals of solidification. Trans. Tech. Publications, 1998.
[49] Yang M, Guo T, Qin C, et al. Microstructure, tensile and creep properties of as-cast Mg-3.8Zn-2.2Ca-*x*Ce (*x*=0, 0.5, 1 and 2 wt.%) magnesium alloys. Journal of Rare Earths, 2012, 30(2): 181–188.
[50] Zhang H, Fan J, Zhang L, et al. Effect of heat treatment on microstructure, mechanical properties and fracture behaviors of sand-cast Mg-4Y-3Nd-1Gd-0.2Zn-0.5Zr alloy. Materials Science and Engineering: A, 2016, 677: 411–420.
[51] Huang Y, Yang L, You S, et al. Unexpected formation of hydrides in heavy rare earth containing magnesium alloys. Journal of Magnesium and Alloys, 2016, 4(3): 173–180.
[52] Yamada K, Okubo Y, Shiono M, et al. Alloy development of high toughness Mg-Gd-Y-Zn-Zr alloys. Materials Transactions, 2006, 47(4): 1066–1070.
[53] Anyanwu I A, Kamado S, Kojima Y. Creep properties of Mg-Gd-Y-Zr alloys. Materials Transactions, 2001, 42(7): 1212–1218.
[54] Wang F, Fu B G, Wang Y F, et al. (Y, Gd)H_2 phase formation in as-cast Mg-6Gd-3Y-0.5Zr alloy. China Foundry, 2021, 18(3): 217–222.
[55] Stulikova I, Smola B, Buch F V, et al. Development of creep resistant Mg-Gd-Sc alloys with low Sc content. Materials Science & Engineering Technology, 2001, 32(1): 20–24.
[56] Apps P, Karimzadeh H, King J, et al. Phase compositions in magnesium-rare earth alloys containing yttrium, gadolinium or dysprosium. Scripta Materialia, 2003, 48(5): 475–481.
[57] Wang J, Fu J, Dong X, et al. Microstructure and mechanical properties of as-cast Mg-Al-Sn-Y-Nd alloy. Materials & Design, 2012, 36: 432–437.